SKB

TECHNICAL REPORT 93-17

Oxidation of uraninite

Janusz Janeczek, Rodney C Ewing

Department of Earth & Planetary Science,
University of New Mexico, Albuquerque, NM, USA

June 1993

SVENSK KÄRNBRÄNSLEHANTERING AB
SWEDISH NUCLEAR FUEL AND WASTE MANAGEMENT CO

BOX 5864 S-102 48 STOCKHOLM

TEL 08-665 28 00 TELEX 13108 SKB S
TELEFAX 08-661 57 19

OXIDATION OF URANINITE

Janusz Janeczek, Rodney C Ewing

Department of Earth & Planetary Science, University of New Mexico, Albuquerque, NM, USA

June 1993

Oxidation of Uraninite

Janusz Janeczek*

Rodney C. Ewing

Department of Earth & Planetary Sciences,
University of New Mexico
Albuquerque, New Mexico 87131, U.S.A.

*presently at
Department of Earth Sciences, Silesian University,
Bedzinska 60, 41-200 Sosnowiec, Poland

June, 1993

Keywords: spent nuclear fuel, uraninite, UO_2, oxidation, corrosion, natural analogue, Cigar Lake.

ABSTRACT

Samples of uraninite and pitchblende annealed at 1200°C in H_2, and untreated pitchblende were sequentially oxidized in air at 180-190°C, 230°C, and 300°C. Uraninite and untreated pitchblende oxidized to the U_4O_9-type oxide, and their x-ray symmetry remained isometric up to 300°C. Reduced pitchblende, after oxidation to UO_{2+x} and U_4O_9-type oxides, transformed into α-U_3O_8 at 300°C. Two major mechanisms control uraninite and untreated pitchblende stability during oxidation: 1) Th and/or lanthanide elements maintain charge balance and block oxygen interstitials near impurity cations; 2) the uraninite structure saturates with respect to excess oxygen and radiation-induced oxygen interstitials. Untreated pitchblende during oxidation behaved similarly to irradiated UO_2 in spent nuclear fuel; whereas, reduced pitchblende resembled non-irradiated UO_2.

An analysis of the data in the literature, as well as our own efforts (XRD, EMPA, SEM, AEM) to identify U_3O_7 in samples from Cigar Lake, Canada, failed to provide conclusive evidence of the natural occurrence of tetragonal α-U_3O_7. Most probably, reported occurrences of U_3O_7 are mixtures of isometric uraninites of slightly different compositions.

ABSTRACT (Swedish)

Prover av uraninit och pechblände glödgade vid 1200°C i H_2 och obehandlad pechblände oxiderades i sekvens i luft vid 180-190°C, 230°C och 300°C. Uraninit och obehandlad pechblände oxiderade till oxider av U_4O_9-typ och deras röntgensymmetri förblev isometrisk upp till 300°C. Reducerad pechblände, efter oxidation till UO_{2+x} och oxider av U_4O_9-typ, omvandlades till α-U_3O_8 vid 300°C. Två huvudmekanismer kontrollerar stabiliteten hos uraninit och obehandlad pechblände under oxidation: 1) Th och/eller lantanider bibehåller laddningsbalansen och blockerar interstitiellt syre nära föroreningskatjonerna; 2) uraninitstrukturen mättas med avseende på överskottssyre och strålningsinducerat interstitiellt syre. Obehandlad pechblände uppförde sig under oxidation på ett sätt liknande bestrålad UO_2 i utbränt kärnbränsle, medan reducerad pechblände liknade obestrålad UO_2.

En analys av litteraturdata såväl som våra egna insatser (XRD, EMPA, SEM, AEM) för att identifiera U_3O_7 i prover från Cigar Lake, Kanada, lyckades inte ge avgörande belägg för natulig förekomst av tetragonal α-U_3O_7. Det troligaste är att rapporterade förekomster av U_3O_7 är blandningar av isometriska uraniniter med något olika sammansättningar.

TABLE OF CONTENTS

SUMMARY

The use of natural uraninite (UO_{2+x}) as an analogue for the long-term corrosion products of the UO_2 in spent nuclear fuel requires the careful analysis of the alteration products of uraninite under experimental and natural conditions. This report presents results of a detailed experimental study of the oxidation products of uraninite and its fine-grained variety, pitchblende. Samples of uraninite and pitchblende annealed at 1200°C in H_2, and untreated pitchblende were sequentially oxidized in air at 180-190°C, 230°C, and 300°C. All samples were analyzed by x-ray diffraction. Uraninite and untreated pitchblende oxidized to the U_4O_9-type oxide, and their x-ray symmetry remained isometric up to 300°C. Reduced pitchblende, after oxidation to UO_{2+x} and U_4O_9-type oxides, transformed into α-U_3O_8 at 300°C.

Two major mechanisms control uraninite and untreated pitchblende stability during oxidation:

1) Th and/or lanthanide elements maintain charge balance and block oxygen interstitials near impurity cations;

2) the uraninite structure saturates with respect to excess oxygen and radiation-induced oxygen interstitials. Untreated pitchblende during oxidation behaved similarly to irradiated UO_2 in spent nuclear fuel; whereas, reduced pitchblende more closely resembled non-irradiated UO_2.

Based on the results of previous studies, we also tried to confirm the occurrence of U_3O_7 in naturally altered samples. An analysis of the data in the literature, as well as our own efforts (x-ray diffraction analysis, electron microprobe analysis, scanning electron microscopy and analytical electron microscopy) to identify U_3O_7 in samples from Cigar Lake, Canada, failed to provide conclusive evidence of the natural occurrence of tetragonal α-U_3O_7. Most probably, reported occurrences of U_3O_7 are mixtures of isometric uraninites of slightly different compositions.

Under oxidizing conditions, the higher oxides of UO_2 (e.g., U_3O_7 or U_3O_8) are unlikely for form in nature due to the presence of water which will cause the formation of uranium oxide hydrates.

1 INTRODUCTION

After extensive investigations in the 1940's and 1950's, uraninite is again of increased interest because of its role as an analogue for UO_2 in spent nuclear fuel [1-4]. Uraninite, nominally UO_2, is nonstoichiometric with a highly defective fluorite structure type. The nonstoichiometry and defects are caused by oxidation of uranium, cation substitution, and α-decay event damage. Therefore, the structural formula of uraninite can be written as [5]:

$$(U^{4+}_{1-x-y-z-u-v}\,U^{6+}_{x}\;\;Th^{4+}_{u}\,REE^{3+}_{y}\;\;M^{2+}_{z}\,\square_{v}{}^{4+})O_{2+x-(0.5y)-z-2v}$$

One of the fundamental problems of uraninite mineralogy is to determine the extent to which uraninite is analogous in chemistry and corrosion behaviour to synthetic UO_2. Part of this problem is addressed by studying the early stages of oxidation of uraninite.

During oxidation of U^{4+} to U^{6+} in UO_2, excess oxygen is incorporated into the structure causing the formation of nonstoichiometric UO_{2+x}, where x is the number of excess interstitial oxygens and is equal to the amount of U^{4+} converted to U^{6+}. At ambient temperatures the limit of solid solution is small, probably less than $x = 0.1$. The UO_{2+x} phase changes to isometric U_4O_9 when the solubility limit is exceeded [6]. The transformation involves long-range ordering of the interstitial oxygens. Oxidation of UO_2 at temperatures below 150°C and up to 250°C results in the formation of two metastable "pseudo-cubic" tetragonal, non-stoichiometric phases, designated α-U_3O_7 and β-U_3O_7, respectively [7,8]. Further oxidation of this material produces orthorhombic U_3O_8. UO_2 ($a = 0.5468$ nm) and α-U_3O_7 ($a = 0.5467$ nm) are practically equidimensional in the **ab**-plane. There are two additional U_3O_7 phases, tetragonal and monoclinic, both high-pressure and high-temperature [9]. The sequence UO_2-U_4O_9 -U_3O_7 has been observed during oxidation of UO_2 at 300°C [10]. Unlike nonirradiated UO_2, the irradiated UO_2 in spent fuel oxidizes below 250°C to hyperstoichiometric U_4O_9 rather than U_3O_7 [11].

In contrast to synthetic UO_2, we have only limited knowledge of the oxidation of uraninite and its variety pitchblende. Previous experiments on the oxidation of uraninite, summarized by Frondel [12], were inconclusive, because samples were heated at temperatures which were too high, e.g. 900°C in the experiments of Brooker and Nuffield [13]; therefore, always producing U_3O_8 independent of the chemical compositions of heated uraninites. In this paper, we present results of the sequential oxidation of two uraninites heated in air at 180-190°C, 230°C, and 300°C. These temperatures were selected to be within the stability fields of α- and β-U_3O_7, and U_3O_8, respectively. We also critically review and discuss reports on the occurrence of natural U_3O_7.

The occurrence of natural, tetragonal α-U_3O_7, has been reported for uranium deposits in Key Lake, Canada [14,15], the Brousse-Broquies Basin, France [16] and Cigar Lake, Canada [17]. Natural U_3O_7 has been accepted in the literature as an end-member of the UO_2-U_3O_7

series [18-20], though it has not been approved by the International Mineralogical Association as a valid mineral species. Natural U_3O_7 has already been proposed as a possible geothermometer [21]. Recent detailed investigations of samples from Key Lake, Canada, have revealed that uraninite is the only uranium oxide present in the deposit, and there is no positive identification of U_3O_7 [22]. In this paper, we show that the data provided in all previous investigations of natural U_3O_7 are insufficient to confirm its occurrence in nature. The existence of natural U_3O_7, especially in deposits considered as natural analogues for geologic repositories of spent nuclear fuel, e.g. Cigar Lake, Canada, is of particular interest because U_3O_7 can be used to define the conditions of uraninite dissolution and alteration.

2 SAMPLE DESCRIPTIONS

The samples in this study were from the research collection of the Department of Earth & Planetary Sciences of the University of New Mexico, and included pegmatitic uraninite from Webb Mine, Mitchell County, North Carolina (sample UNM336) and hydrothermal uraninite (pitchblende) from Jàchymov, Czechoslovakia (sample UNM430; = Harvard Museum #96537). We also analysed uraninite (pitchblende) from Cigar Lake (sample CS620), Canada, from which crystals of "U_3O_7" had been reported [23]. Uraninite from the Webb Mine occurs as black, well developed cubo-octahedral crystals. The Jàchymov specimen is black and massive and cut by a network of calcite veinlets. Uraninite from the Webb Mine pegmatite is moderately rich in Th; whereas, pitchblende from Jàchymov is Th-free (Table 1). Appreciable amounts of Y+REE have been detected in both samples. The chemical ages of uraninites from Webb Mine and Jàchymov, estimated from the content of Pb determined by electron microprobe analyses (Table 1), are 387 and 188 million years (Ma), respectively. A relatively high silica content (>1 wt.%) in Jàchymov pitchblende is typical for this locality and may result from the presence of small amounts of submicroscopic coffinite, $USiO_4$, abundant in Jàchymov [24], although x-ray diffraction analysis did not reveal any coffinite diffraction maxima in sample 430. Coffinite was also not detected in back scattered electron images. There is a substantial amount of CaO (>5 wt.%) in the chemical analysis of pitchblende from Jàchymov (Table 1). Calcium can substitute for uranium in the uraninite structure, creating an oxygen vacancy to compensate for the loss of positive charge.

The uraninite from Webb Mine is a single-phase sample as revealed by the x-ray powder diffraction analysis (Table 2). Pitchblende from Jàchymov was poorly crystalline and contained at least two uranium oxides as suggested by the x-ray diffraction pattern (Fig. 2). Therefore, d-spacings and the unit-cell parameter reported in Table 2 represent mean values. The densities of the samples from Webb Mine, 9.42 gcm^{-3}, and Jàchymov, 6.65 gcm^{-3}, are 86% and only 61%, respectively, of the theoretical density of UO_2 (10.952 gcm^{-3}). The low density of #430 probably results from poor crystallinity, the presence of water (suggested by the low total in the electron microprobe analysis), the presence of low-density impurities, e.g. calcite, or the presence of voids and fractures associated with the accumulation of helium due to radioactive decay.

Table 1. Electron microprobe data (wt%) for uraninite from Webb Mine (sample 336) and from Jachymov (sample 430) [24].

	336	430
UO_2	87.39	81.54
ThO_2	2.23	0.00
SiO_2	0.00	1.23
ZrO_2	0.27	0.02
PbO	4.30	1.93
CaO	0.32	5.30
Y_2O_3	1.09	0.70
La_2O_3	0.13	n.d.
Ce_2O_3	0.23	0.54
Gd_2O_3	0.52	0.10
Na_2O	0.20	0.00
P_2O_5	0.00	0.14
Total	96.68	91.50

Table 2. X-ray powder diffraction data (dcal and dobs, nm x 10^{-1}; I/Io - relative intensity; Ipk-top - intensity measured at the maximum of the diffraction peak, cps; FWHM - full width at the half maximum of the peak) for uraninite from Webb Mine and pitchblende from Jàchymov.

Webb Mine						Jàchymov				
dcal	dobs	I/Io	Ipk-top	FWHM	hkl	dcal	dobs	I/Io	Ipk-top	FWHM
3.156	3.16	100	18334	0.250	111	3.131	3.13	100	4644	0.730
2.733	2.74	37	6730	0.233	200	2.711	2.71	34	1559	0.608
1.933	1.934	34	6271	0.347	220	1.917	1.917	36	1660	0.960
1.648	1.648	26	4794	0.431	311	1.635	1.635	26	1228	0.911
1.578	1.578	6	1080	0.408	222	1.565	1.565	3	150	0.722
1.366	1.366	5	996	0.390	400	1.356	1.359	3	145	0.801
1.254	1.254	9	1683	0.631	331	1.244	1.244	5	246	0.976
1.222	1.222	6	1136	0.589	420					
1.116	1.116	6	1115	0.731	422					
1.052	1.052	6	1032	0.704	511					
0.966	0.967	1	286	0.644	440					
a = 0.54664(3) nm						a = 0.54229(4) nm				

3 EXPERIMENTAL TECHNIQUES

Powdered samples 336 and 430 were annealed in H_2 for 24 hours at 1200°C in an Astro Ultra-High Temperature tube furnace in order to reduce the U^{6+} apparently present in uraninites. The samples and an aliquot of untreated sample 430 (subsample 430B) were then heated in convecting air at 180°C in two stages for periods totaling 48 hours. The samples were subsequently oxidized in static air at 230°C for 72 hours and at 300°C for 65 hours.

After each heating run, the samples were examined by x-ray powder diffraction using a Scintag diffractometer and $CuK_{\alpha 1}$ radiation. Data were collected in the multi-range step scan mode with step size 0.025° 2Θ. Counts were collected for 6 s at each point. The width of the receiving slit was 0.5 mm. A silicon NBS SRM standard was used as an external standard. Background subtraction and a $K_{\alpha 2}$ stripping routine (Scintag software) were applied in the data reduction. Unit cell parameters were refined using a least-squares routine (NIST LSQ85 program).

Electron microprobe analyses of untreated samples were performed using the JEOL 733 Superprobe operated at an accelerating voltage of 15 kV and a sample current of 20 nA. The data were reduced using Bence-Albee correction procedures (Sandia Task 8 program). Synthetic UO_2, and $REEPO_4$, and minerals (cerussite for Pb, thorite for Th, andesine for Ca, and garnet for Si) were used as standards.

The densities of small chips of uraninite (masses ranged from 5 to 9 mg) were measured in toluene with a Berman balance.

Scanning electron microscopy of sample CS620 from Cigar Lake, Canada, was performed using a Hitachi S-800 field emission scanning electron microscope operated at an accelerating voltage of 15kV. Secondary electron resolution (maximum beam size) was 2 nm. Transmission electron microscopy was performed on the same sample using a JEOL 2000FX operated at 200 kV.

4 RESULTS

Uraninite (sample 336) and pitchblende (sample 430) responded differently to the annealing at 1200°C in a strongly reducing atmosphere. While the unit-cell parameter of sample 336 decreased by 7.5×10^{-2} %, the unit-cell parameter of sample 430 increased by 0.80 % to the value (0.54665(3) nm) close to the unit-cell parameter of pure UO_2 (0.5470 nm) (Table 3). This is consistent with previous annealing studies of uraninite [25] and pitchblendes [26] in a reducing atmosphere. The contraction of the unit cell of uraninite results from annealing of the radiation-induced defects, in agreement with experiments on irradiated UO_2 [27-29]. Expansion of the unit cell of pitchblende was predominantly due to the reduction of U^{6+} to U^{4+} [26]. The intensity of the x-ray diffraction peaks of sample 430 increased dramatically. For example, the intensity of the strongest uraninite peak, 111 (d = 0.315 nm), increased from 4644 cps to 32573 cps. At the same time, the full width at the half maximum (FWHM) of the peak decreased from 0.730 to 0.129. Because the crystallinity of sample 336 was initially much higher than the crystallinity of sample 430 (Table 2), the increase in intensity of the diffraction peaks was not so dramatic. Even so, the intensities

increased on average by 200%. For instance, the intensity of the 111 peak increased from 18334 cps to 55735 cps. The increase in intensity was associated with a decrease in FWHM, predominantly due to the reduction of strain and recrystallization as suggested by the Williamson-Hall plot (Fig. 1). The Williamson-Hall plot separates the peak broadening due to strain from that caused by decreased crystallite size. Density increased from 9.42 to 9.78 gcm^{-3} in sample 336 and from 6.65 to 7.63 gcm^{-3} in sample 430.

Table 3. Unit cell parameters a_o (nm) and density D ($g\ cm^{-3}$) of uraninite from Webb Mine (sample 336) and pitchblende from Jáchymov (samples 430 and 430B)

Sample	336		430		430B
	a_o	D	a_o	D	a_o
untreated	0.54645(3)	9.42	0.54229(4)	6.65	0.54229(4)
1200°C, H_2, 24h	0.54604(3)	9.78	0.54665(3)	7.63	
190°C, air, 24h	0.54576(2)	9.84	0.54688(2) 0.5456(1)	7.44	0.5401(4)
190°C, air, 48h	0.54594(2)	9.78	0.5463(2) 0.5422(2)	7.72	0.5403(9)
230°C, air, 72h	0.54557(4) 0.54354(8)	9.78	0.54656(4) 0.5452(1) 0.5410(5)	7.59	0.5401(4)
300°C, air, 68h	0.54352(6)				0.5404(1)

Oxidation of sample 336 in air at 180-190°C resulted in a decrease in the unit-cell parameter (Table 3) but no other phase formed. The density increased to 9.84 gcm^{-3} (+4.5 %). This suggests an O/M ratio of 2.005. Extension of the heating time at 190°C to another 24 hours resulted in a slight increase in the unit-cell parameter (Table 3) but no change in mass was observed. The density, however, decreased to 9.78 gcm^{-3}, i.e. reached the value of the sample annealed at 1200°C in H_2.

After heating sample 430 at 180-190°C for 24 hours, all peaks on the x-ray diffraction patterns displayed high-angle tailing (Fig. 2). This indicates partial oxidation of the sample, most probably, to the cubic U_4O_9 structure. Peaks were decomposed, and both sets of peaks were indexed in the *Fm3m* space group. Unit-cell parameters of both phases were significantly larger than the unit cell-parameter of an untreated sample (Table 3). The position of the high-angle, low-intensity peaks in sample 430 after heating at 190°C coincides with the mean position of the diffraction peaks of the untreated sample. Some peaks were split, and the splitting was enhanced after additional heating at 190°C (Fig. 2b). These observations suggest the presence of a minor phase with a lower symmetry than isometric (possibly tetragonal α-U_3O_7). However, another explanation is also plausible. Annealing of sample 430 in H_2 reduced the uraninite. Yet, careful analysis of the background revealed the presence of weak peaks at the 2Θ-angles related to the peaks of untreated sample 430. This suggests that either the reduction of uraninite was not complete

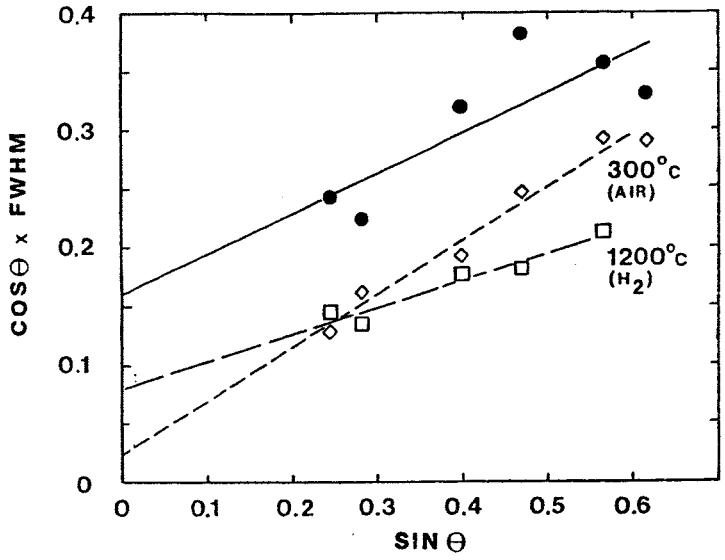

Figure 1. Williamson-Hall plot for uraninite from Webb Mine untreated, annealed at 1200°C in H_2, and heated in air at 300°C. Slopes of the lines are proportional to the strain, and intercepts are inversely proportional to the crystallite size.

after 24 hours of annealing or these weak peaks resulted from the incongruent decomposition of uraninite into UO_{2+x} and U_4O_9 which may have occurred at temperatures lower than 1200°C, followed by an incomplete homogenization of the system at 1200°C [26]. In this case, the peaks would be due to the remnants of U_4O_9 . These small crystallites may have served as nuclei for the formation of $U_4O_{9\pm x}$ phases at 190°C.

The unit-cell parameter of subsample 430B decreased by 0.4% after heating at 190°C in air (Table 3). The quality of the x-ray diffraction pattern, already poor for the untreated sample, further deteriorated (intensities of the diffraction maxima decreased and FWHM increased). Heating at 190°C for another 24 hours did not change the unit cell parameter within the precision limit (Table 3). Broad and weak diffraction maxima of the heated sample 430B are indicative of small crystallite size.

After annealing at 230°C, two phases formed in sample 336. Decomposed x-ray diffraction peaks could be assigned to two cubic phases, both with unit cells smaller than the original unit cell of sample 336 (Table 3). The density did not change on heating, and there was only the slight increase in mass of the sample (0.03%). The intensity of x-ray diffraction maxima increased, but the peaks broadened significantly.

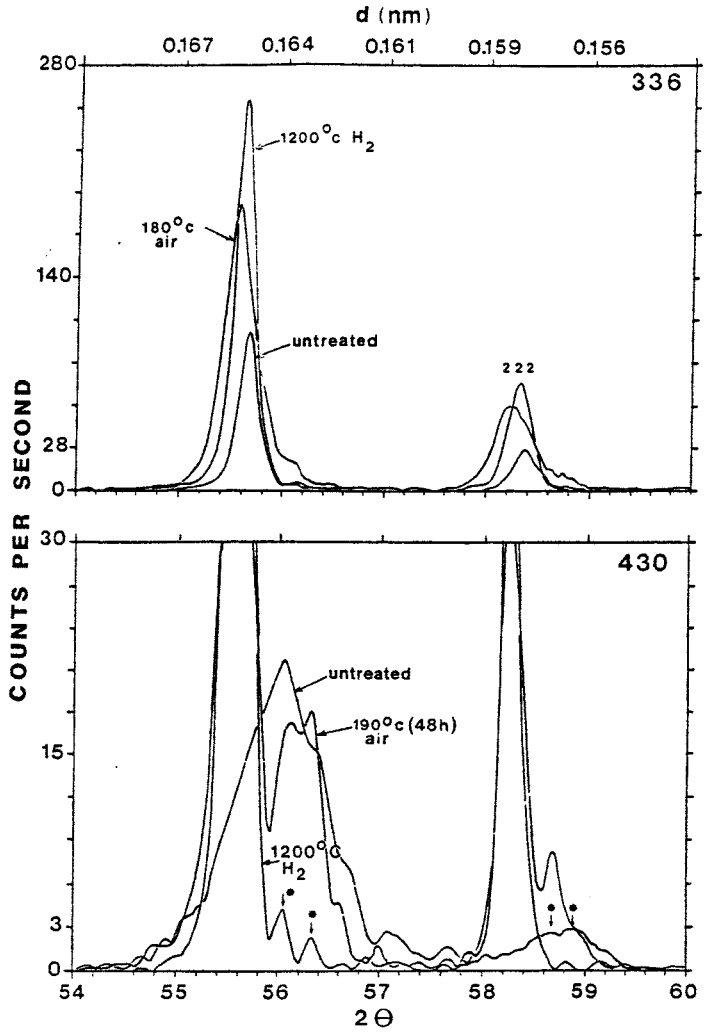

Figure 2. Peak profiles of the 311 and 222 diffraction maxima of uraninites from (a) Webb Mine (#336) and (b)Jachymov (#430) before heating and after heating at 1200°C in H_2 and 190°C in air. Peaks with "*" indicate diffraction features that may be interpreted as relicts of the original (unannealed) structure (#430).

After heating sample 430 at 230°C, x-ray diffraction peaks were decomposed into three components (including 111 and 222 peaks). This suggests the presence of three cubic phases (Fig. 3, Table 3). The density decreased to 7.59 gcm^{-3}. The difference between the unit cell parameter of the reduced sample 430 and a mean unit cell parameter of the sample annealed at 230°C (Δ = 0.03 Å) is similar to the difference between untreated sample 430 and the oxidized sample 430B (Δ = 0.02 Å) and is the same as the difference between the reduced sample 336 and sample oxidized at 230°C (Δ = 0.03 Å).

Annealing sample 336 at 300°C did not result in significant changes. The quality of the x-ray pattern deteriorated, however, due to peak broadening and a decrease in peak intensities. The increase in slope on the Williamson-Hall plot (Fig. 1) suggests that the peak broadening was caused by increased strain during oxidation. The presence of two phases in the sample was no longer obvious, because decomposition of most peaks could not be completed unambiguously, and certain peaks could not be decomposed at all.

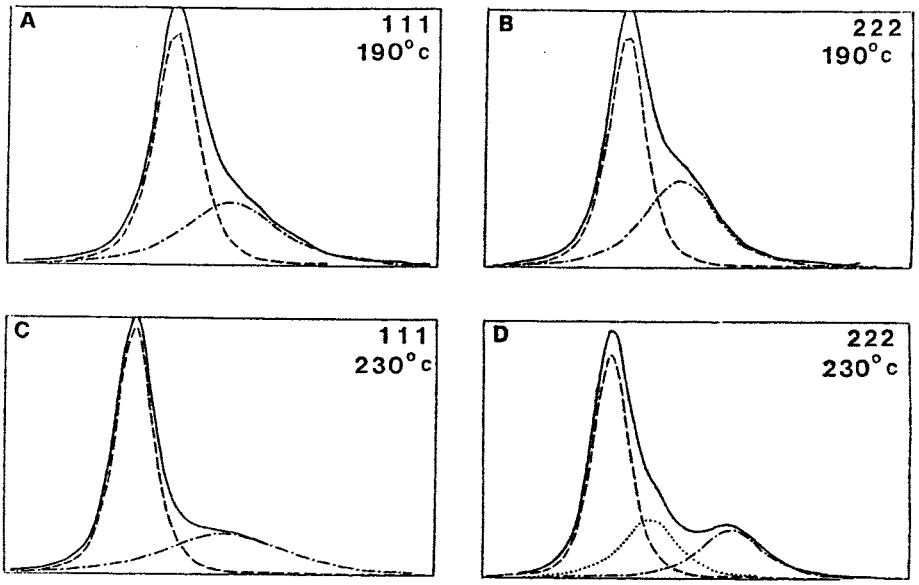

Figure 3. Decomposition of the 111 and 222 peaks of pitchblende from Jachymov heated in air at 190°C (a,c) and 230°C (b,d).

Table 4. X-ray powder diffraction data for synthetic α-U_3O_7 and uranium oxides from the Key Lake and Brousse-Broquies Basin.

	1	2	3	4	5	6	7	8	9
hkl	dobs	dobs	dcalT	dcalC1	dcalC2	dobs	dcalT	dcalC1	dcalC2
111	3.14	3.14	3.143	3.145	3.121	3.10	3.112	3.139R	3.119
200	2.723	2.72	2.734R	2.724		2.72	2.691R	2.718	
002	2.696	2.70	2.697		2.703	2.70	2.702		2.701
220	1.926	1.928	1.933R	1.926		1.92	1.907R	1.922	
202	1.918	1.918	1.920		1.911R	1.91	1.903		1.910R
311	1.645	1.63	1.647	1.642		1.64	1.629R	1.639	
113	1.628	1.63	1.630		1.630	1.62	1.624		1.628
222	1.567			1.572	1.560			1.569	1.559
a_T,nm	0.5472		0.5468(4)				0.538(3)		
c_T,nm	0.5397		0.5394(4)				0.540(2)		
c/a	0.986		0.986				1.004		
a_1,nm				0.5447(5)				0.5436(3)	
a_2,nm					0.5405(2)				0.5402(1)

Note: 1 - α-U_3O_7 (Westrum and Grønvold, 1962); 2 - Sample from Key Lake (Voultsidis and Classen, 1978); 3 - d-values calculated for tetragonal phase; 4 - d-values calculated for isometric phase I; 5 - d-values calculated for isometric phase II; 6 - Sample from the Brousse-Broquies Basin (George et al., 1986); 7 - d-values calculated for tetragonal phase; 8 - d-values calculated for isometric phase I; 9 - d-values calculated for isometric phase II
d-values in nm x 10
R - peaks rejected by the algorithm during unit cell refinement

Annealing of sample 430 at 300°C resulted in the break down of the uraninite structure and crystallization of α-U_3O_8. The process of transformation was not completed, however, as indicated by the presence of weak peaks of uraninite on the x-ray diffraction pattern. During this process the mass of sample 430 increased by 0.25%. The color of the sample changed from black to olive-green with black streaks. Small pieces of the sample, that had been used for the density measurements, turned into powder in the crucible due to the dramatic increase in volume. The volume of α-U_3O_8 is 1.36 relative to UO_2. Stacking disorder in the layered structure of U_3O_8 is indicated by a significant broadening of peaks other than 001 and 002 (Fig. 4). Unit cell parameters of α-U_3O_8 are: **a** = 0.673(1) nm, **b** = 1.197(2) nm, **c** = 0.414(1) nm. Annealing of sample 430B at 300°C did not result in a phase transformation, and the isometric phase persisted (Fig. 4). No change in the mass of the sample was observed.

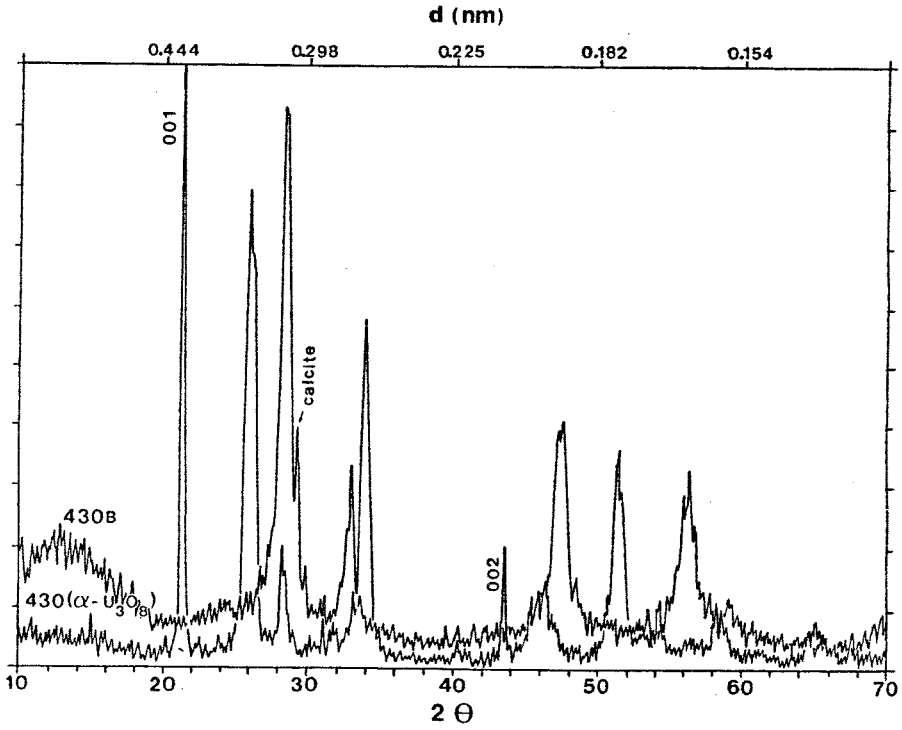

Figure 4. X-ray diffraction patterns of samples 430 and 430B oxidized in air at 300°C. Sample 430 transformed into α-U_3O_8; whereas, sample 430B remained an isometric uraninite. Note the sharp 001 and 002 peaks on the x-ray pattern of α-U_3O_8 in sample 430 in contrast to the broadening of other peaks.

5 DISCUSSION

5.1 OXIDATION OF URANINITE

Uraninite and untreated pitchblende oxidized to the U_4O_9-structure type and remained isometric up to 300°C; whereas, reduced pitchblende transformed into α-U_3O_8 at this temperature. During low-temperature oxidation, uraninite and reduced pitchblende

decomposed to two or even three cubic phases, that apparently differed in the degree of oxidation up to the composition of U_4O_9. In none of these uraninites was it possible to detect with certainty, on the basis of x-ray powder diffraction analysis, the deviation from isometric symmetry. Certainly, kinetics play an important role in the formation of U_3O_7. In the experiments on the oxidation of UO_2 pellets in air after 70 h oxidation at 230°C, UO_2 remained cubic with the unit cell parameter as low as 0.5395(4) nm [30]. After 139 h oxidation of UO_2, a tetragonal distortion was observed. Taylor et al. [8] observed that in the early stages of oxidation, the $UO_{2.33}$ (U_3O_7) peaks could be indexed on the basis of a cubic unit cell, with a = 0.539 nm. Interestingly, these small values of the unit-cell parameter coincide with the smallest unit-cell parameters reported for pitchblende from Jachymov, i.e. 0.5385-0.539 nm [26,31]. Perhaps, a prolonged oxidation of uraninite produces a lower-symmetry oxide, at least in the reduced sample 430. The resistance of reduced uraninite and untreated Th-free pitchblende to the formation of higher oxides, i.e. U_3O_7 and U_3O_8, in these experiments implies two different mechanisms may inhibit oxygen diffusion. In pegmatitic uraninite, the presence of Th played a key role in the stabilization of isometric symmetry. Thorium is always tetravalent; therefore, it repels positively charged oxygen vacancies, thus limiting the number of oxygen interstitials that can enter the uraninite structure. The effect of rare-earth elements (REE), frequently found in uraninites from pegmatites, has been demonstrated for UO_2-$La(Y)_2O_3$ solid solutions [32]. During oxidation of these materials, the fluorite structure was retained with a reduction in the unit-cell parameter. A consideration of the role of impurities (e.g., Pb^{2+} and Ca^{2+}) in the structure of uraninite suggests that the amount of excess oxygen required to compensate for the increasingly positive charge resulting from oxidation of U^{4+} to U^{6+} is less than tha suggested by the amount of U^{6+} alone [5]. Therefore, greater amounts of U^{4+} can be converted to U^{6+} in uraninite with impurities than in pure UO_{2+x} without causing the displacive transformation of the isometric structure to tetragonal or orthorombic structures [5]. In addition to the requirement of charge neutrality, the blocked interstitial oxygen sites in the vicinity of an impurity cation are the main cause of the increase in the oxygen potential of the mixed uranium oxides as compared to pure UO_{2+x} [33].

The different behaviors of reduced pitchblende 430 and untreated sample 430B during oxidation at 300°C require another mechanism, as both samples initially had the same chemical composition and a highly defective structure prior to heating. Heating sample 430 in H_2, resulted in reduction of U^{6+} to U^{4+}, recrystallization, and annealing of defects. Untreated sample 430B contained some U^{6+} and excess oxygens. Heating in air at 190°C further oxidized the sample, which caused contraction of the unit cell and an increase in strain in the structure, seen as peak-broadening on the x-ray diffraction pattern, but no observable changes in the x-ray diffraction symmetry. Further heating, up to 300°C, did not result in significant changes. This implies a rather high rate of oxidation. The oxidation was enhanced by the small grain size in the untreated sample (large surface area). There is probably a "saturation" level of excess oxygen in UO_{2+x} that stabilizes the isometric structure until, at sufficiently high temperature and/or P_{O_2}, the UO_{2+x} oxidizes to U_3O_8. This is illustrated by the behavior of UO_{2+x} with $x < 0.38$ that

retained an isometric structure after heating at 150-350°C, but it oxidized rapidly to U_3O_8 above 350°C [34]. Einziger et al. [11] observed that the transition of irradiated UO_2 with oxygen to a metal:oxygen ratio of 2.42 (i.e., U_4O_{9+x}) was inhibited at 250°C. At temperatures above 280°C, the oxidation proceeded rapidly to U_3O_8. Irradiated UO_2 in spent fuel formed U_4O_{9+x} particulates at weight gains significantly higher than those for non-irradiated fuel [35]. The fact that both natural uraninite and irradiated UO_2 maintained the isometric symmetry longer than reduced uraninite and non-irradiated UO_2 suggests that the concentration and mobility of radiation-induced point defects may also play an important role in suppressing oxygen diffusion into the oxide structure. Irradiation of UO_2 causes the formation of anion Frenkel defects and, at higher doses, formation of Schottky-type and extended defects. At temperatures below 400°C, oxygen interstitials are mobile in the irradiated UO_2 [28] and in uraninites [25,26]. The formation of oxygen interstitials during the neutron irradiation or α-decay events may inhibit oxygen diffusion into the oxide structure by reducing the number of interstitial sites available for excess oxygen.

Dry oxidation of uraninite is unlikely to occur in nature, because of the presence of water that would lead (partly due to the radiolysis of water) to the formation (in the absence of other cations) of uranium oxide hydrates, i.e. schoepite (UO_3 $2H_2O$) or ianthinite ($U^{4+}(UO_2)_5(OH)_{14}$ $3H_2O$)[36,37]. This has also been demonstrated in experiments in which UO_2 was oxidized to UO_3 hydrates in air-steam mixtures above 50% saturation, near 200°C [38]. Possible mechanisms for these transformations in natural systems have recently been discussed by Finch and Ewing [36,37].

Some comments on the oxidation state of natural uraninites are appropriate to this discussion. According to commonly accepted models for uraninite formation, uranium is transported by oxidizing solutions as U^{6+}. When these solutions attain reducing conditions, U^{6+} is reduced to U^{4+} which results in precipitation of uraninite. To explain the observation that uraninite always contains some U^{6+}, post-formational oxidation has been assumed. The absence of pure UO_2 in nature prompted Frondel [12] to suggest that "...uraninite may crystallize directly in a more or less oxidized condition...". This suggestion is supported by the presence of trivalent and divalent cations in uraninite that must have coprecipitated with uranium. If during crystallization uranium was only tetravalent, the incorporation of impurity cations would result in a substoichiometric oxide. This is highly unlikely. If, however, U^{6+} was available, the charge balance could be maintained and only a small amount of excess oxygen would enter the uraninite structure. At low temperatures, there is only a limited solid solution of oxygen in UO_2 ($UO_{2.04}$-$UO_{2.07}$) [9]; thus, post-formational, partial oxidation of U^{4+} is difficult. Pegmatitic and hydrothermal uraninites form at 300-500°C [39] which is the stability field of UO_{2+x} and β-U_4O_{9-y} for $x < 0.25$ (depending on composition of the system) [9]. Therefore, it is reasonable to expect that, at least in this temperature range, uraninite can precipitate as a complex $U^{4+}U^{6+}$-oxide.

5.2 NATURAL U_3O_7

The tetragonal symmetry of reported natural uranium oxides has been based on x-ray powder diffraction data. The diffraction maxima of the x-ray diffraction patterns for samples from Key Lake and the Brousse-Broquies Basin were composed of "doublets" with the exception of the 111 peak. George et al. [16] reasoned that the split peaks could not be the result of a mixture of two isometric uraninites (with different unit cell parameters) because the 111 peak was undivided. This argument is, however, not compelling when one considers the angular dependence of the resolution of x-ray diffraction maxima. Resolution decreases with decreasing 2Θ angle. Thus, overlapping peaks are much more easily resolved at higher values of 2Θ. For isometric phases with similar unit cell parameters, diffraction maxima will not be resolved at low angles of 2Θ. As an example, uraninite from Musunoi, Zaire has overlapping peaks that are readily decomposed at high angles of 2Θ. The calculated unit-cell parameters for both isometric phases are $\mathbf{a_1}$ = 0.54583(6) nm and $\mathbf{a_2}$ = 0.5442(2) nm [26]. Because $\Delta 2\Theta_{111}$ is small (= 0.09°), the 111 peak at 28.4° 2Θ is not resolved, but it is noticeably wider than the 111 peak of single phase uraninite. The presence of two uraninites, with slightly different compositions, in the sample from Musunoi has been confirmed directly by electron microprobe analyses and back scattered electron imaging [26]. If the difference in unit-cell parameters between two uraninites is large, it may be possible to observe evidence of the overlapping of the two 111 peaks. In the x-ray diffraction data of Kish and Cuney [40], the 111 and 200 peaks have distinct high-angle shoulders. Diffraction maxima at higher angles of 2Θ are clearly resolved. The difference in the unit-cell parameters between the two uraninites in this pattern is 0.0034 nm and $\Delta 2\Theta_{111}$ = 0.18°, twice that observed in the uraninite from Musunoi. If the diffraction maxima are broadened due to strain or small crystallite size (common in uraninite), they may not be resolved even at larger values of $\Delta 2\Theta$. The resolution of the diffraction maxima also depends on instrumental parameters such as receiving slit width, step scan mode, counting time, and scan rate. In order to avoid ambiguities in the interpretation of x-ray diffraction data of uranium oxides (particularly to distinguish between mixtures of isometric phases and a tetragonal phase), the analysis should concentrate on the 222 peak at approximately 58.8° $2\Theta_{Cu}$ (d_{222} = 0.1567 nm). For the tetragonal phase none of the nX(111) peaks should be split. Unfortunately, the x-ray diffraction patterns for the samples from Key Lake and Brousse-Broquies do not cover this important 2Θ region.

X-ray diffraction results showing high angle tailing of uraninite peaks in samples from Cigar Lake were also originally interpreted as evidence of α-U_3O_7 [17]. Broadening and high-angle tailing of the uraninite 222 peak were observed, but were attributed to small crystallite size. After further analysis, Sunder et al. [43] concluded that the uraninite peaks in the Cigar Lake samples were too broad to distinguish between tetragonal U_3O_7 and a mixture of isometric uraninites having slightly different lattice parameters.

Using the x-ray diffraction data of Voultsidis and Clasen [15] and George et al. [16], unit-cell parameters were calculated for tetragonal and isometric unit cells. In the latter case, it was assumed that the material consisted of two isometric phases with overlapping 111

peaks. In some cases (Table 4), there was a higher precision in the calculated unit cell parameters for the isometric unit cells; and the $d_{calculated}$ matched the $d_{observed}$ for the isometric unit cells better than for the tetragonal unit cell.

Results from X-ray photoelectron spectroscopy have been used to confirm the presence of U_3O_7 in the Cigar Lake deposit [17]. The values of the U^{6+}/U^{4+} ratio (0.24 - 0.57), calculated from high-resolution X-ray photoelectron spectra, suggest a composition close to U_3O_7 ($UO_{2.19\text{-}2.36}$). However, the number of excess oxygens (x) in UO_{2+x} can be estimated from the U^{6+}/U^{4+} ratio only for pure uranium oxides. In the presence of other cations that may enter the uraninite structure, either as interstitial defects or in substitution for uranium, the charge balance requirements may change the stoichiometry. As an example, the recalculation of the chemical analysis provided by George et al. [16] gives x = 0.32, that suggests a composition of U_3O_7 ($UO_{2.33}$), only if elements other than uranium (e.g., . Ca) are excluded from the calculations and the analysis is normalized to 100 percent for UO_2 and UO_3. If, however, in addition to uranium, Ca is taken into account (CaO = 4.1 wt.%) the value of x is as low as 0.07, and the formula of the uraninite may be written as:

$$(U^{4+}_{0.55}U^{6+}_{0.26}Ca^{2+}_{0.19})O_{2.07}.$$

In both calculations, the U^{6+}/U^{4+} ratio is 0.48. Thus, the U^{6+}/U^{4+} ratios derived from XPS analyses cannot be used to determine the excess oxygen content in uraninite unless impurities are absent.

Many uraninites display anomalous birefringence or optical anisotropy [22]. This indicates a lower optical symmetry, a common phenomenon among minerals with well known examples in garnet and beryl. The anomalous birefringence in uraninite may be caused by internal strain due to cation substitutions or oxidation, interstitial substitution, radiation-induced defects, or crystal growth defects. A strong anisotropy due to strain has been detected in pitchblendes [26]. Uraninite crystals from Key Lake are intimately twinned [22]; thus strain may be the cause of their optical anisotropy. Deviation from optical isotropy by uraninite can occur independently from its oxidation state, i.e., with any composition of UO_{2+x}; therefore, this does not necessarily indicate the presence of U_3O_7. However, the tetragonal oxide must be optically anisotropic. George et al. [16] explained the absence of optical anisotropy in their "tetragonal" sample as due to the "pseudo-cubic nature of the crystal" or its partial metamictization. Neither explanation is substantive.

George et al. [16] refers to the tetragonal symmetry of crystals seen by SEM. The SEM micrographs are not conclusive and could just as easily be interpreted as uranium oxide pseudomorphs after coffinite (tetragonal $USiO_4$), a replacement feature not uncommon in uranium deposits. In fact, it is possible to make a direct comparison between the SEM images in the paper of George et al. [16] and coffinite crystal forms [41]. Cramer et al. [23] reproduced the SEM micrograph of sample (CS620) from Cigar Lake that showed well developed, tetragonal crystals 1 μm in size. EDS and WDS spectra obtained from these crystals showed the presence of only U and O. Cramer et al. [23] suggest that these are crystals of tetragonal uranium oxide. However, the habit of these crystals is identical to the crystal of coffinite shown in the same paper. During our investigation of

sample CS620 by X-ray powder diffraction and scanning electron microscopy, we found crystals with a habit identical to that shown by Cramer et al. [23] (Fig. 5a). The EDS spectrum of these crystals (Fig. 5b) revealed U as a major element, a strong signal from Si, and weak signals from Al, Ca, and Pb. Thus, the SEM results suggest that the crystals are a uranium silicate, e.g., coffinite. This was confirmed by x-ray powder diffraction analysis.

To determine whether the uraninite from Cigar lake actually contained α-U_3O_7 or a mixture of compositionally distinct uraninites, a sample (CS620-B3) was examined by analytical transmission electron microscopy (TEM). Previous analysis of companion samples from the same drill core section by x-ray photoelectron spectroscopy indicated U^{+6}/U^{+4} ratios of about 0.7 [43]. Unlike x-ray diffraction, electron diffraction usually lacks the angular resolution needed to distinguish tetragonal U_3O_7 from isometric fluorites (UO_2 and U_4O_9) having slightly different lattice parameters. However, electrons are strongly scattered by oxygen atoms, and the characteristic ordering of excess oxygen in U_4O_9 is indicated by superlattice spots or diffuse-scattering in the electron diffraction patterns [44]. Based on the neutron diffraction results of Masaki [45], similar oxygen ordering occurs in U_3O_7. Although several modifications of U_3O_7 and U_4O_9 are known [42, 44], the presence of extra electron diffraction maxima produced by ordered excess oxygen in the basic fluorite lattice is sufficient for identification. Selected-area electron diffraction was used to examine uraninite regions as small as ~0.2 μm in diameter for the oxygen-excess phases. Convergent-beam electron diffraction (CBED) in principle offers better angular resolution than the selected-area method, and might be used to directly identify uraninite phases by symmetry or lattice parameter differences. However, the CBED method proved inapplicable because of the highly strained state of the uraninite. Local uraninite areas excited by a 20 to 30 nm electron probe were also analyzed for compositional differences by energy-dispersive x-ray spectrometry (EDS).

The TEM sample was prepared from a petrographic thin section containing mostly uraninite with coffinite and clay along fine cracks and vugs. After re-embedding the section with epoxy, a uraninite region was selectively thinned by dimple grinding and 5 keV argon ion milling. Both surfaces were finished by milling at 2 keV and an incident beam angle of ~4° to remove most of the "black spot" damage produced by ion bombardment. Previous experience with TEM of oxidized uranium oxides has shown that neither ion milling nor exposure to 120 to 200 keV electrons alters the structure of U_4O_9 or U_3O_7 unless the sample is accidentally heated.

Examination of the Cigar Lake sample showed no U_4O_9 or U_3O_7, but revealed the presence of two distinct uraninites--one coarse-grained and lead-rich, and the other extremely fine-grained and lead-poor. By analogy with Pb-rich and Pb-poor uraninites previously identified by scanning electron microscopy and electron microprobe analysis in a sample from Musunoi [26], the two uraninites are respectively termed type I and II. The uranium minerals occurred in an apparent alteration sequence, with fine-grained type II uraninite surrounding much larger (10 to 100 μm) grains of type I material and grading into coarse-grained coffinite ($USiO_4$) near cracks. A uranium-rich clay was further associated with the coffinite.

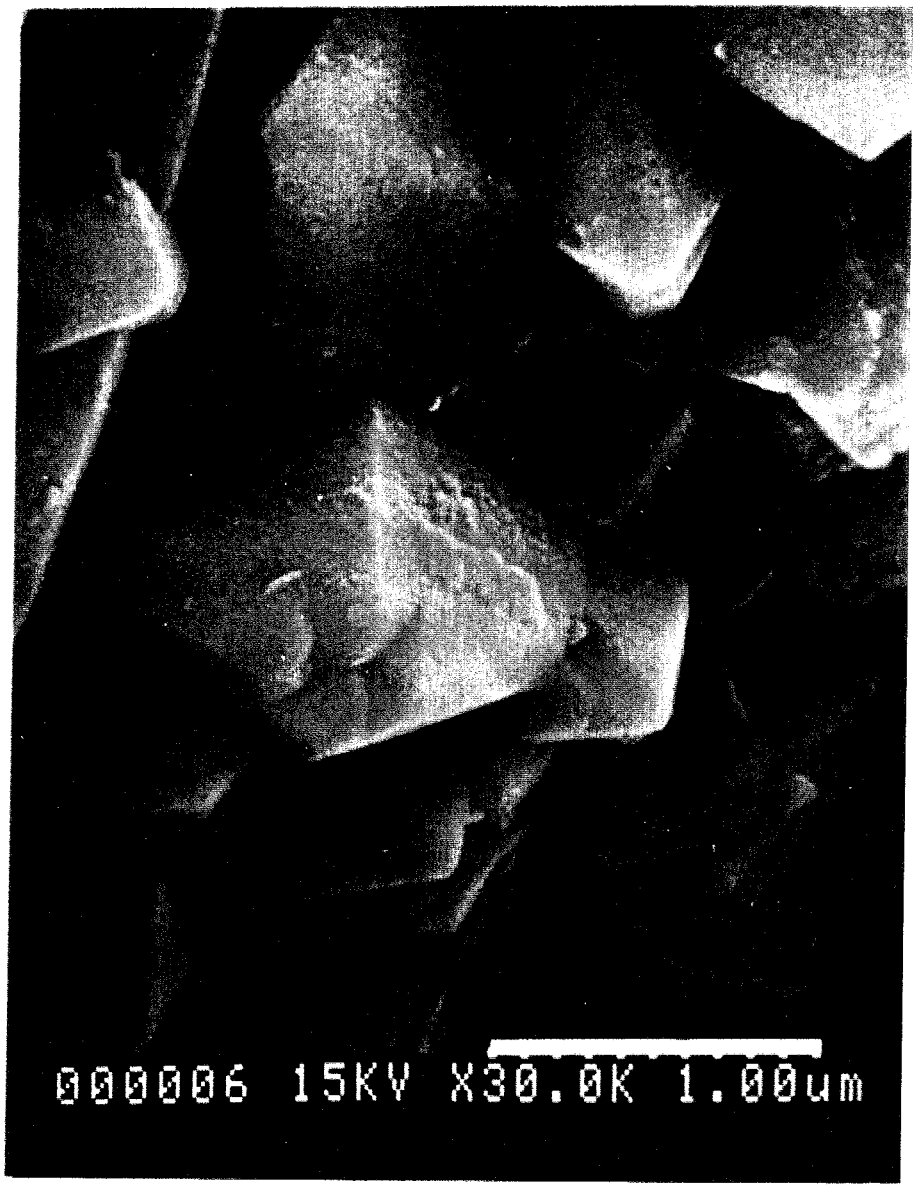

Figure 5a. SEM micrograph of crystals lining a vug in sample CS620 from Cigar Lake. Scale bar 1 μ m.

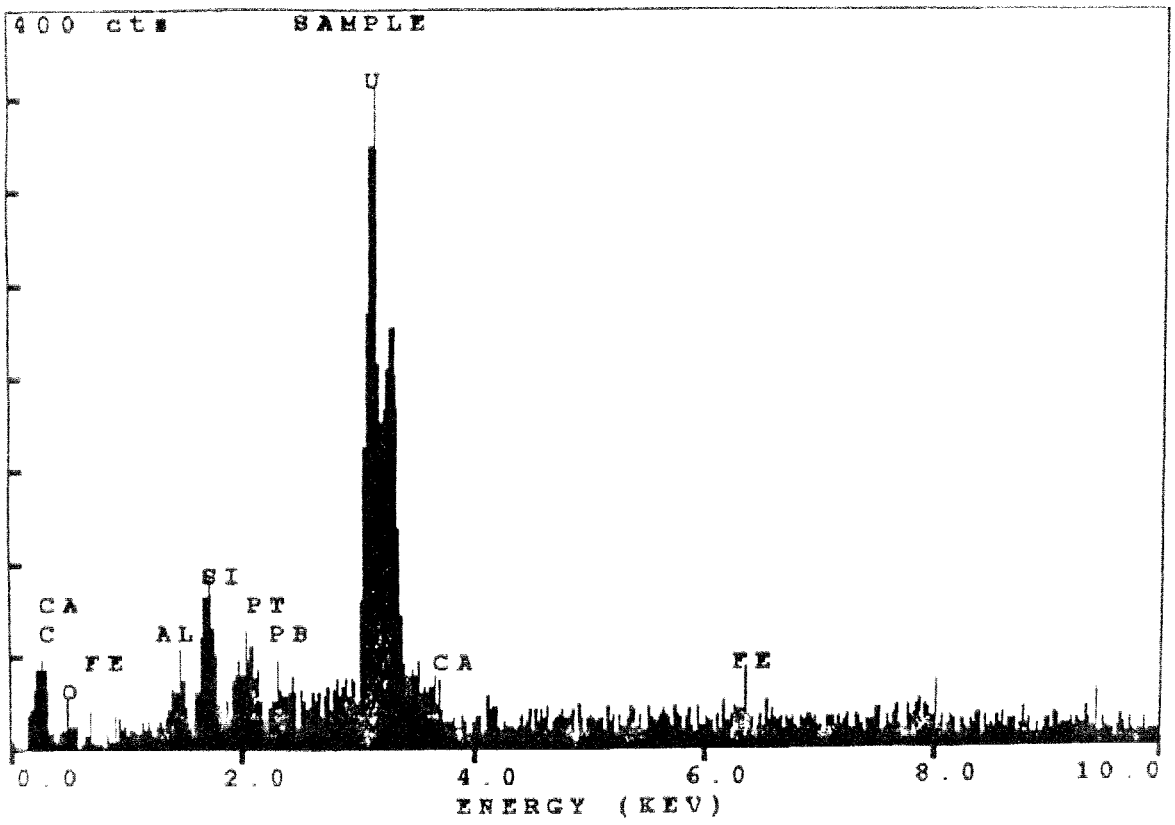

Figure 5b. EDS spectrum of coffinite crystals lining a vug in sample CS620 from Cigar Lake. Counting time was 600 s.

Figure 6 shows the microstructure and corresponding selected-area diffraction patterns from a contact region between uraninite I and II. The coarse and fine-grained uraninites shared an abrupt interface with no detectable intermixing and gave spot or ring diffraction patterns containing only fundamental UO_2 diffraction maxima. Sizes of the type II grains measured from darkfield micrographs varied from 1 to 20 nm. Micrographs of type I grains taken under strong diffracting conditions showed extensive dislocation substructures and other evidence of high strains. The highly strained nature of the type I uraninite was also indicated by asterism (spot streaking) and a lack of sharp Kikuchi lines in the diffraction patterns. Although both uraninites contained scattered 0.1 to 1 μm particles of mostly galena (PbS), regions between the particles generally appeared precipitate-free and produced no detectable precipitate diffraction maxima. Judging from the absence of detectable superlattice spots or diffuse scattering maxima in the diffraction patterns, neither uraninite contained U_3O_7 or U_4O_9. Both uraninites apparently had UO_2 structures with no ordered excess oxygen.

Microbeam EDS analyses revealed large differences in lead and silicon contents of the coarse- and fine-grained uraninites. Representative spectra of the two uraninites and coffinite are shown for comparison in Figure 7, and results of "standardless" analyses are given in Table 5. Apart from minor titanium in both uraninites, and yttrium in the coffinite, other elements heavier than sodium (Z = 11) in these minerals were at or below detection limits of approximately 0.5 wt%. These analyses contain many approximations, but gave results that are consistent with quantitative analysis results obtained from similar samples by x-ray photoelectron spectrometry and electron microprobe analysis. The mechanism by which apparently precipitate-free regions of uraninite can incorporate Pb and Si concentrations far above expected solubility limits is unexplained. A compositional profile (Figure 8) obtained by stepping a 30 nm electron probe across the uraninite I/II interface shown in Figure 6 indicates the abrupt change in Pb and Si concentrations at the interface.

The observations of two compositionally different uraninites having (isometric) UO_2 structures, one uraninite highly strained and the other with extremely small crystallite size, are also consistent with the reported peak broadening and high-angle tailing noted in x-ray diffraction studies. Based on these observations, the presence of α-U_3O_7 in the Cigar Lake sample examined is unlikely. The uraninites in this sample appear to be UO_2 solid solutions containing U^{+6} due to impurity charge compensation, but with oxygen below its solubility limit in the UO_2 structure.

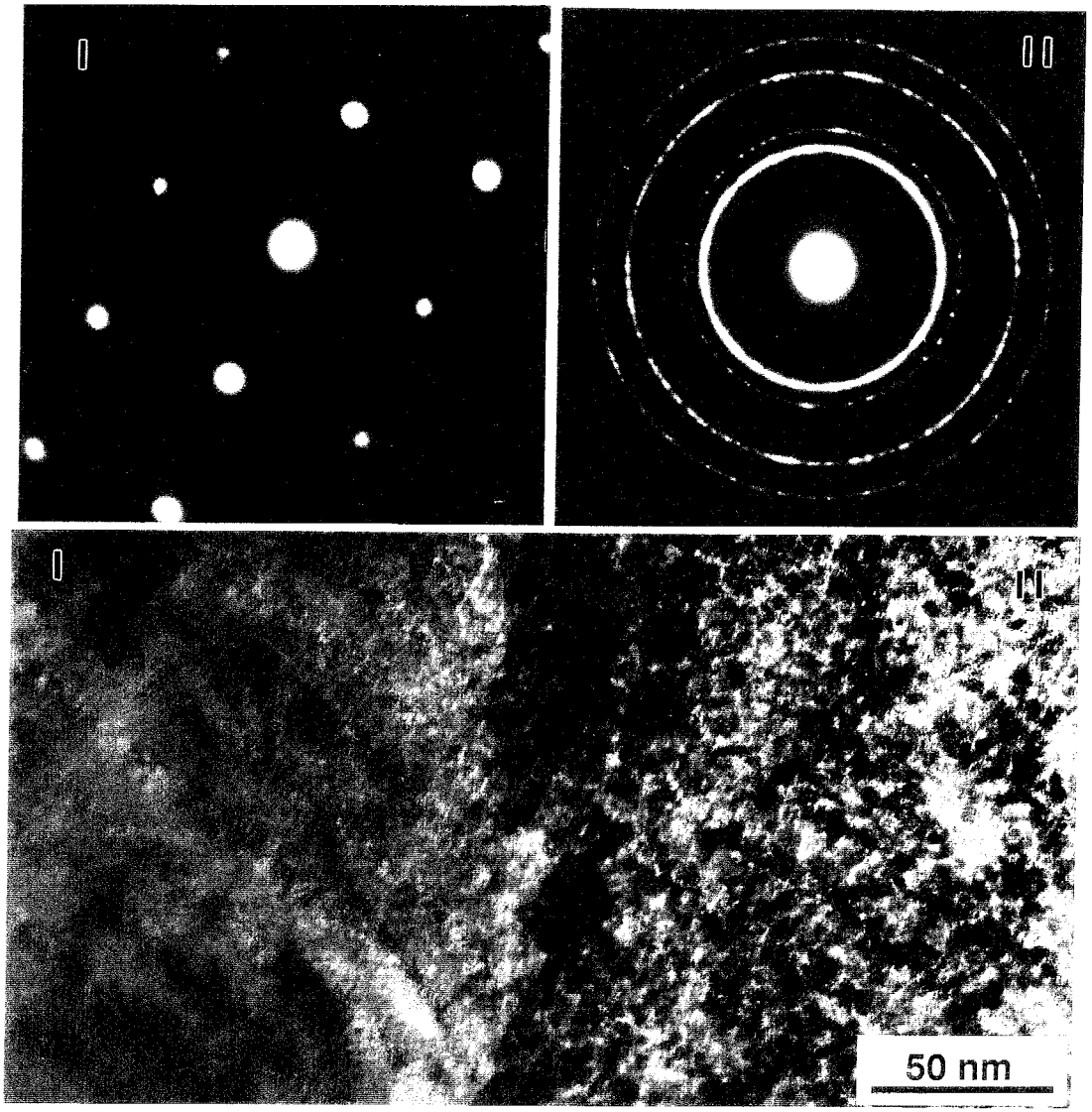

Figure 6. Interface region between uraninite-I and -II, with selected-area diffraction patterns from adjacent coarse- and fine-grained material. Cigar Lake sample CS-620. Only fundamental diffraction maxima of the UO_2 fluorite-structure (not U_3O_7 or U_4O_9) were detected. Dislocations in the highly strained uraninite-I do not appear in this micrograph.

Table 5. EDS microbeam analysis (wt. %) of U-phases at Cigar Lake.

Element	uraninite-I	uraninite-II	coffinite
Si	0.8	3.1	12.0
Ti	0.8	1.2	-.-
Y	-.-	-.-	2.1
Pb	16.1	1.4	-.-
U	82.3	94.3	85.9

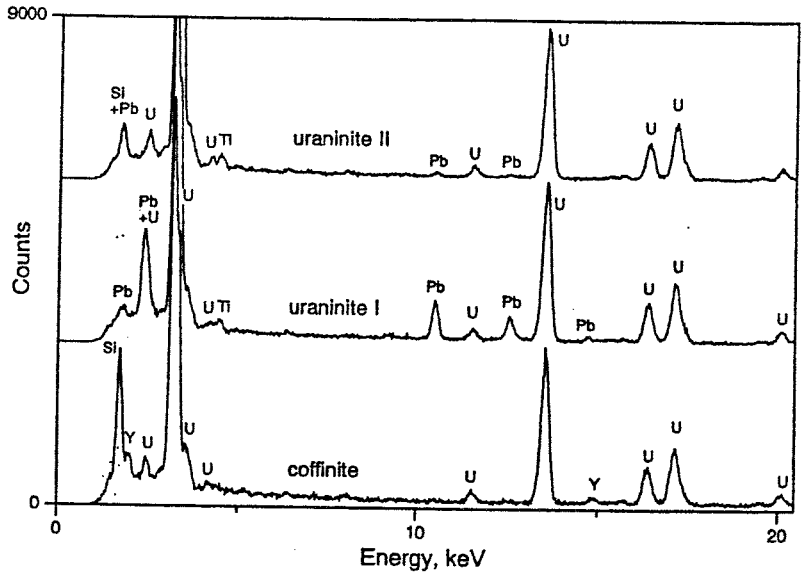

Figure 7. EDS spectra from precipitate-free regions of uraninite and coffinite in Cigar Lake sample CS-620. 200 keV electrons.

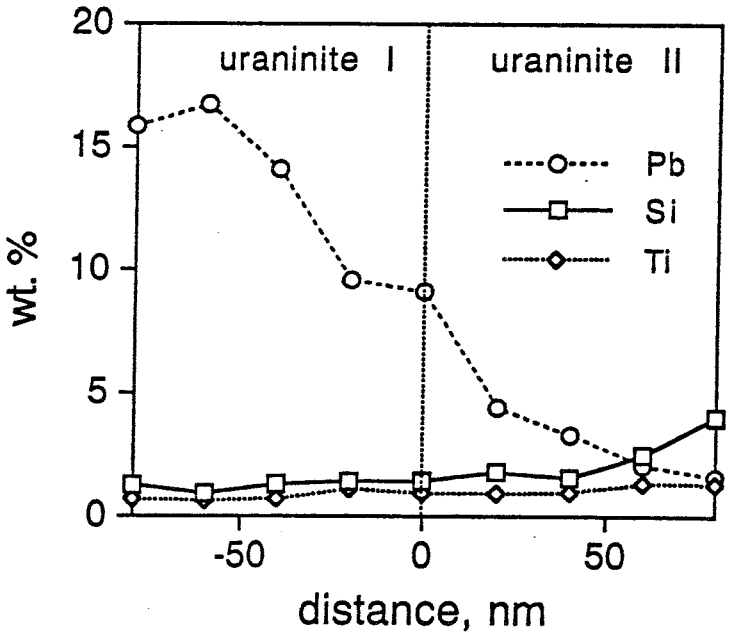

Figure 8. EDS composition profile across uraninite I/II interface in Fig. 6. Profile may be broadened by probe size (~30 nm) and inclination of interface.

6 CONCLUSIONS

The oxidation path of uraninite depends on the uraninite chemistry and structure. Two major mechanisms control uraninite stability during early stages of oxidation:

1) Th and/or lanthanide elements maintain charge balance and "block" oxygen interstitial movement near impurity cations; thus, enabling U^{4+} oxidation with limited incorporation of excess oxygen into the uraninite structure;

2) the isometric uraninite structure saturates with respect to excess oxygen and radiation-induced oxygen interstitials. Sufficient temperature and/or P_{O_2} will transform the isometric structure into orthorhombic U_3O_8. This process is unlikely to occur in nature, because of the presence of water that causes the formation of uranium oxide hydrates. Uraninite appears to be a better analogue of dry, irradiated UO_2 in spent fuel than of non-irradiated UO_2.

An analysis of data in the literature, as well as our own efforts to identify U_3O_7 in samples from Cigar Lake, Canada, has failed to provide conclusive evidence of tetragonal α-U_3O_7 in natural samples. Most probably, reported occurrences of U_3O_7 are mixtures of isometric uraninites with slightly different compositions. This is an important observation, because of the proposed role of α-U_3O_7 in geochemical models of the long-term corrosion of the UO_2 in spent nuclear fuel.

7 ACKNOWLEDGMENTS

This work was supported by the Swedish Nuclear Fuel and Waste Management Co. and, in its latter stages, the U.S. Nuclear Regulatory Commission. We thank Mark Miller for technical assistance with SEM and XRD analysis. The manuscript benefited from extended discussions with Jan Cramer, Bob Finch, Sham Sunder, and Peter Taylor. Special thanks are due to Larry Thomas of Battelle PNL for his analytical electron microscopy. Sample 430 (HM 96537) was obtained from the Harvard Museum courtesy of Carl Francis, and sample 336 was donated to the UNM research collections by Gregory Lumpkin. Sample CS620 was obtained through the courtesy of Jan Cramer as part of the research program of the Cigar Lake Natural Analogue Project sponsored by AECL (Canada), SKB (Sweden) and US/DOE (USA). The electron microprobe analyses and x-ray diffraction study were completed in the Electron Microbeam Analysis Facility of the Department of Earth and Planetary Sciences and the Institute of Meteoritics of the University of New Mexico.

8 REFERENCES

[1] L.H. Johnson and D.W. Shoesmith in: Radioactive Waste Forms for the Future, Eds. W. Lutze and R.C. Ewing (Elsevier, Amsterdam, 1988) p. 635.

[2] R.C. Ewing, in: Proceedings of the Third International Symposium on Advanced Nuclear Energy Research (1991), 167.

[3] R.J. Finch and R.C. Ewing, SKB Technical Report 91-15 (1991).

[4] J. Janeczek and R.C. Ewing, J. Nucl. Mater. 190 (1992) 157.

[5] J. Janeczek and R.C. Ewing, J. Nucl. Mater. 190 (1992) 128.

[6] E.H.P. Cordfunke, The Chemistry of Uranium. (Elsevier, Amsterdam, 1969).

[7] H.R. Hoekstra, A. Santoro and S. Siegel, J. Inorg. Nucl. Chem. 18 (1961) 166.

[8] P. Taylor, E.A. Burgess and D.G. Owen, J. Nucl. Mater. 88 (1980) 153.

[9] D.K. Smith, B.E. Scheetz, C.A.F. Anderson and K.L. Smith, Uranium 1 (1982) 79.

[10] S.R. Teixeira and K. Imakuma, J. Nucl. Mater. 178 (1991) 33.

[11] R.E. Einziger, L.E. Thomas, H.C. Buchanan and R.B. Stout, J. Nucl. Mater. 190 (1992) 53.

[12] C. Frondel, Geol. Surv. Bull. 1064 (1958) p. 400.

[13] E.J. Brooker and E.W Nuffield, Amer. Mineral. 37 (1952) 363.

[14] F.J. Dahlkamp. Econ. Geol. 73 (1978) 1430.

[15] V. Voultsidis and D. Classen, Erzmetall 31 (1978) 8.

[16] E. George, M. Pagel, Y. Dusausoy and J.M. Gautier, Uranium 3 (1986) 69.

[17] S. Sunder, P. Taylor and J.J. Cramer, Mater. Res. Soc. Symp. Proc. 112, (1988) 465.

[18] H.R Steacy and S. Kaiman, in: Short Course in Uranium Deposits: Their Mineralogy and Origin. Mineral. Asoc. Can., (Toronto, 1978) 107.

[19] J.B. Maynard, Geochemistry of Sedimentary Ore Deposits, (Springer, Berlin, 1983) p. 295.

[20] D.K.Jr. Smith, in: Uranium Geochemistry, Mineralogy, Geology, Exploration and Resources, Eds. B. de Vivo, F. Ippolito, G. Capaldi, and P.R. Simpson (Institution of Mining and Metallurgy, London, 1984) p. 43.

[21] V. Voultsidis, von E. Pechmann, and D. Clasen, in: G.C. Amstutz, A. El Goresy, G. Frenzel, and G. Moh, Eds., Ore Genesis - The State of the Art, Springer, Berlin, 1982) p. 469.

[22] von E. Pechmann, H. Hürter, H-J. Bernhardt, and R. Fritsche, in M. Cuney et al. Eds., Primary Radioactive Minerals (Theophrastus Publications, Athens, 1991) p. 335.

[23] J. Cramer, S. Sunder and P. Taylor in: AECL/SKB/USDOE Cigar Lake Project. Progress report for the period May-October 1991. (AECL Research, Pinawa, 1991) p.38.

[24] J. Janeczek, N. Jb. Miner. Mt. 9 (1991) 385.

[25] P.J. Stout, G.R. Lumpkin, R.C. Ewing, and Y. Eyal, Mater. Res. Soc. Symp. Proc. 112 (1988) 495.

[26] J. Janeczek and R.C. Ewing, J. Nucl. Mater. 185 (1991) 66.

[27] N. Nakae, Y. Iwata and T. Kirihara, J. Nucl. Mater. 80 (1979) 314.

[28] W.J. Weber, J. Nucl. Mater. 114 (1983) 213.

[29] W.J. Weber, Rad. Effects 83 (1984) 145.

[30] P.A. Tempest, P.M. Tucker and J.W. Tyler, J. Nucl. Mater. 151 (1988) 251.

[31] M. Cathelineau, M. Cuney, J.Leroy, F. Lhote, C. Nguyen Trung, M. Pagel and B. Poty, in: Vein-type and Similar Uranium Deposits in Rocks Younger than Proterozoic. Proc. Technical Committee

Meeting, Lisbon 24-28 September 1979, (IAEA Vienna, 1982) p. 159.
[32] W.B. Wilson, C.A. Alexander and A.F. Gerds, J. Inorg. Nucl. Chem. 20 (1961) 242.
[33] K. Park and D.R. Olander, J. Nucl. Mater. 187 (1992) 89.
[34] V.A. Alekseyev, L.A. Ana'yeva, and R.P. Rafal'skiy, Internat. Geol. Rev. 23 (1979) 1229.
[35] T.K. Campbell, E.R. Gilbert, C.K. Thornhill, and B.J. Wrona, Nucl. Technol. 84 (1989) 182.
[36] R.J. Finch and R.C. Ewing, in: Scientific Basis for Nuclear Waste Management XIV, Eds. T. Abrajamo and L.H. Johnson, Mater. Res. Soc. Symp. Proc. 212 (1991) 241.
[37] R.J. Finch and R.C. Ewing, J. Nucl. Mater. 190 (1992) 133.
[38] P. Taylor, D.D. Wood, A.M. Duclos and D.G. Owen, J. Nucl. mater. 168 (1989) 70.
[39] R. Rich, H.D. Holland and U. Petersen, Hydrothermal Uranium Deposits. Developments in Geology, 6 (Elsevier, Amsterdam, Oxford, New York, 1977)
[40] L. Kish and M. Cuney, Min. Mag. 44 (1981) 473.
[41] Yu.M. Dymkov, Priroda Uranovoi Smolianoi Rudy. (Atomizdat, Moskva, 1973) (in Russian).
[42] E. F. Westrum and F. Gronvold, J. Phys. Chem. Sol. 23 (1962) 39.
[43] S. Sunder, J.J. Cramer, and N.H. Miller, Mater. Res. Soc. Symp. Proc. 257 (1992) 449.
[44] H. Blank and C. Ronchi, Acta Cryst. A24 (1968) 657.
[45] N. Masaki, J. Nucl. Mater. 101 (1981) 229.

List of SKB reports

Annual Reports

1977-78
TR 121
KBS Technical Reports 1 – 120
Summaries
Stockholm, May 1979

1979
TR 79-28
The KBS Annual Report 1979
KBS Technical Reports 79-01 – 79-27
Summaries
Stockholm, March 1980

1980
TR 80-26
The KBS Annual Report 1980
KBS Technical Reports 80-01 – 80-25
Summaries
Stockholm, March 1981

1981
TR 81-17
The KBS Annual Report 1981
KBS Technical Reports 81-01 – 81-16
Summaries
Stockholm, April 1982

1982
TR 82-28
The KBS Annual Report 1982
KBS Technical Reports 82-01 – 82-27
Summaries
Stockholm, July 1983

1983
TR 83-77
The KBS Annual Report 1983
KBS Technical Reports 83-01 – 83-76
Summaries
Stockholm, June 1984

1984
TR 85-01
Annual Research and Development Report 1984
Including Summaries of Technical Reports Issued during 1984. (Technical Reports 84-01 – 84-19)
Stockholm, June 1985

1985
TR 85-20
Annual Research and Development Report 1985
Including Summaries of Technical Reports Issued during 1985. (Technical Reports 85-01 – 85-19)
Stockholm, May 1986

1986
TR 86-31
SKB Annual Report 1986
Including Summaries of Technical Reports Issued during 1986
Stockholm, May 1987

1987
TR 87-33
SKB Annual Report 1987
Including Summaries of Technical Reports Issued during 1987
Stockholm, May 1988

1988
TR 88-32
SKB Annual Report 1988
Including Summaries of Technical Reports Issued during 1988
Stockholm, May 1989

1989
TR 89-40
SKB Annual Report 1989
Including Summaries of Technical Reports Issued during 1989
Stockholm, May 1990

1990
TR 90-46
SKB Annual Report 1990
Including Summaries of Technical Reports Issued during 1990
Stockholm, May 1991

1991
TR 91-64
SKB Annual Report 1991
Including Summaries of Technical Reports Issued during 1991
Stockholm, April 1992

1992
TR 92-46
SKB Annual Report 1992
Including Summaries of Technical Reports Issued during 1992
Stockholm, May 1993

Technical Reports
List of SKB Technical Reports 1993

TR 93-01
Stress redistribution and void growth in butt-welded canisters for spent nuclear fuel
B L Josefson[1], L Karlsson[2], H-Å Häggblad[2]
[1] Division of Solid Mechanics, Chalmers University of Technology, Göteborg, Sweden
[2] Division of Computer Aided Design, Luleå University of Technology, Luleå, Sweden
February 1993

TR 93-02
Hydrothermal field test with French candidate clay embedding steel heater in the Stripa mine
R Pusch[1], O Karnland[1], A Lajudie[2], J Lechelle[2], A Bouchet[3]
[1] Clay Technology AB, Sweden
[2] CEA, France
[3] Etude Recherche Materiaux (ERM), France
December 1992

TR 93-03
MX 80 clay exposed to high temperatures and gamma radiation
R Pusch[1], O Karnland[1], A Lajudie[2], A Decarreau[3],
[1] Clay Technology AB, Sweden
[2] CEA, France
[3] Univ. de Poitiers, France
December 1992

TR 93-04
Project on Alternative Systems Study (PASS).
Final report
October 1992

TR 93-05
Studies of natural analogues and geological systems.
Their importance to performance assessment.
Fredrik Brandberg[1], Bertil Grundfelt[1], Lars Olof Höglund[1], Fred Karlsson[2],
Kristina Skagius[1], John Smellie[3]
[1] KEMAKTA Konsult AB
[2] SKB
[3] Conterra AB
April 1993

TR 93-06
Mineralogy, geochemistry and petrophysics of red coloured granite adjacent to fractures
Thomas Eliasson
Chalmers University of Technology and University of Göteborg, Department of Geology, Göteborg, Sweden
March 1993

TR 93-07
Modelling the redox front movement in a KBS-3 nuclear waste repository
L Romero, L Moreno, I Neretnieks
Department of Chemical Engineering,
Royal Institute of Technology, Stockholm, Sweden
May 1993

TR 93-08
Äspö Hard Rock Laboratory
Annual Report 1992
SKB
April 1993

TR 93-09
Verification of the geostatistical inference code INFERENS, Version 1.1, and demonstration using data from Finnsjön
Joel Geier
Golder Geosystem AB, Uppsala
June 1993

TR 93-10
Mechanisms and consequences of creep in the nearfield rock of a KBS3 repository
Roland Pusch, Harald Hökmark
Clay Technology AB, Lund, Sweden
December 1992

TR 93-11
Post-glacial faulting in the Lansjärv area, Northern Sweden.
Comments from the expert group on a field visit at the Molberget post-glacial fault area, 1991
Roy Stanfors (ed.)[1], Lars O Ericsson (ed.)[2]
[1] R S Consulting AB
[2] SKB
May 1993

TR 93-12
Possible strategies for geoscientific classification for high-level waste repository site selection
Lars Rosén, Gunnar Gustafson
Department of Geology, Chalmers University of Technology and University of Göteborg
June 1993

TR 93-13
A review of the seismotectonics of Sweden
Robert Muir Wood
EQE International Ltd, Warrington, Cheshire, England
April 1993

TR 93-14

Simulation of the European ice sheet through the last glacial cycle and prediction of future glaciation

G S Boulton, A Payne
Department of Geology and Geophysics,
Edinburgh University, Grant Insitute, Edinburgh,
United Kingdom
December 1992

TR 93-15

Analysis of the regional groundwater flow in the Finnsjön area

Anders Boghammar, Bertil Grundfelt, Hans Widén
Kemakta Konsult AB
June 1993

TR 93-16

Kinetic modelling of bentonite – canister interaction.
Implications for Cu, Fe, and Pb corrosion in a repository for spent nuclear fuel

Paul Wersin, Jordi Bruno, Kastriot Spahiu
MBT Tecnologia Ambiental, Cerdanyola, Spain
June 1993